Characterization on Hydrodynamic Behavior in Liquid-Containing Gas-Solid Fluidized Bed Reactor

Yefeng Zhou, Congjing Ren, Jingdai Wang, and Yongrong Yang
State Key Laboratory of Chemical Engineering, Dept. of Chemical and Biological Engineering, Zhejiang University, Hangzhou 310027, PR China

DOI 10.1002/aic.13883
Published online July 23, 2012 in Wiley Online Library (wileyonlinelibrary.com).

In many industrial processes involving gas–solid fluidized bed rectors, the addition of a liquid phase significantly alters the hydrodynamics. To fully characterize the hydrodynamics in the fluidized bed, pressure and acoustic measuring techniques were applied to study the behavior of gas bubbles and particles. A camera was used to take pictures to verify the pressure and acoustic results. During the liquid-addition process, the pressure technique captured the bubble size variation and bubble motion while the acoustic technique reflected particle motion and particle size growth. Hurst and V-statistics analyses of acoustic emission were used for the first time to detect periodic behavior during the injection process. The new break formation and change trend of V_{max} were used as the criteria to judge occurrence of abnormal fluidization states, such as agglomeration and gas channeling formation. These measurement techniques are beneficial in the elimination of adverse effects caused by the addition of liquid. © 2012 American Institute of Chemical Engineers *AIChE J,* 59: 1056–1065, 2013

Keywords: gas–solid fluidized bed, liquid addition, pressure measurement, acoustic emission, hydrodynamic behavior

Introduction

A liquid phase is often introduced into gas–solid fluidized bed reactors (FBRs) in many industrial operations and it plays different roles in different reaction systems. For example, in the condensation mode operation of gas-phase olefin polymerization process, the recycling condensed liquid evaporates under high temperature condition and removes most of heat of reaction in the FBR. In this particular application, the liquid phase aids the heat removal capacity as well as productivity. In the fluidized bed dryer, moisture is evaporated whilst in the fluid coking units or catalytic crackers, the saturated liquid hydrocarbons undergo reactions. However, in some instances the addition of liquid into FBRs negatively affects the quality of fluidization. For example, the increase in moisture content or liquid load may lead to poor mixing, local defluidization and the decrease of fluidization quality, which would result in poor performance of the reactor capability in terms of heat- and mass-transfer, and even worse, may cause catastrophic loss of fluidization. Agglomeration, a commonly encountered problem in the liquid-containing industrial processes perhaps presents the greatest concern. In addition to the increasing importance of liquid-containing gas–solid fluidized beds, the adverse effects posed by input of liquid on fluidization characteristics have drawn a great deal of attention from researchers. Tsujimoto et al.[1] used acoustic emission (AE) sensor technique to detect the onset of unstable fluidization caused by the increase of moisture content in a fluidized bed granulator. McDougall et al.[2,3] investigated the effects of liquid properties on fluidity and agglomerating tendency of fluidized bed, and discovered that the viscosity and contact angle of liquid are two important parameters, directly influencing formation of agglomeration. Weber et al.[4,5] studied the effects of many fluidized bed properties on agglomerates behavior comprehensively, such as characteristics of particle, liquid, and agglomerate. Recently, Book et al.[6] used avalanche test method and vibration measurements to monitor bed fluidity in a wet fluidized bed. Based on the attractor comparison method, Vervloet et al.[7] compared the detection effects of three different sensors (pressure, microphone, and accelerometer) on gradual changeable moisture content, and pointed out that the pressure fluctuation measurements were found to be much better in terms of reproducibility.

Until now, many researchers have focused on the fluidity and stability detection in liquid-containing gas–solid fluidized beds, and from the literature surveyed only a few detailed studies of the hydrodynamic behavior in such kind of fluidized beds have been conducted.[8–10] Because of the significance of such kind of research, further studies are required. In recent years, many measurement techniques have been applied to study hydrodynamics of gas–solid fluidized beds, including direct visualization methods, optical probes, tomography, X-ray imaging, pressure and acoustic measurements.[11–14] However, no individual measurement technique is able to fully characterize hydrodynamics of gas–solid fluidized beds. According to fluidization engineering principles, gas and particle behaviors together determine fluidization characteristics. Therefore, it is crucial to characterize behaviors of gas bubbles and particles so as to study hydrodynamics and

Correspondence concerning this article should be addressed to Jingdai Wang at wangjd@zju.edu.cn.

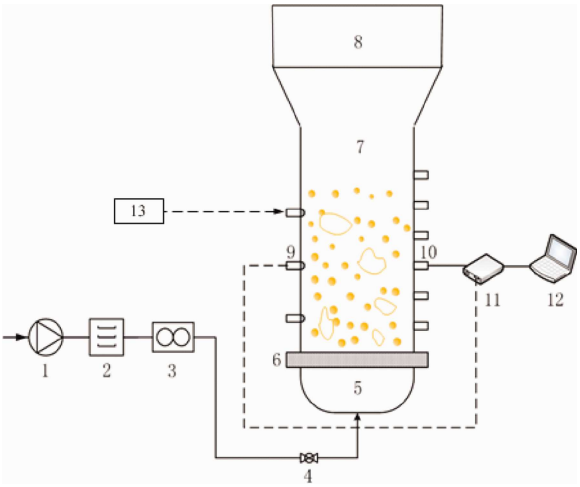

Figure 1. Schematic diagram of the experimental apparatus.

(1) Fan, (2) dryer, (3) flowmeter, (4) ball valve, (5) wind box, (6) gas distributor, (7) fluidized bed, (8) expanding section, (9) pressure transducer, (10) acoustic sensor, (11) signal collection and analysis system, (12) computer, and (13) liquid addition system. [Color figure can be viewed in the online issue, which is available at wileyonlinelibrary.com.]

fluidization characteristics. Compared to other techniques, pressure measurement develops rapidly and can clearly reflect gas bubble behavior in fluidized beds, which has been regarded as a popular and mature measurement technique.[13,15–17] Besides, as a promising technique, AE measurement has received extensive attention in recent years and enjoys a bright future in particle characterization as well as bubble behavior.[18–25] The study of He[26] shows that pressure measurement is suitable for reflecting gas bubble behavior while AE technique is more suitable for characterization of particles and agglomerates motion. Therefore, if both techniques could be combined effectively, hydrodynamic behavior of gas–solid fluidized bed can be better characterized, which also provides a new research perspective for the study of hydrodynamics in liquid-containing gas-solid fluidized beds.

In this article, two main techniques, pressure measurement and AE measurement, are both applied to study hydrodynamics in a lab-scale liquid-containing fluidized bed. Both measurements are analyzed by time domain and frequency domain signal analysis methods from following aspects: standard deviation, power spectrum, wavelet analysis, Hurst analysis, and *V*-statistics analysis. The results of both measurements are verified by images taken with a camera. Gas bubble and particle motion are the main focuses of this research. Obtaining such kind of information will be very beneficial to fully comprehend the problems encountered in the industrial reactors. Through the mentioned techniques and methods, we attempt to achieve the goal of this research, that is, to investigate how the addition of liquid affects hydrodynamics and fluidization characteristics (including gas bubble and particle behavior) of the fluidized bed.

Experimentation

Figure 1 is the schematic diagram of experimental apparatus used in this study. It consists of two main parts: a fluidized bed system and a signal measurement system (pressure or AE measurement system).

The fluidized bed is made of Plexiglas, 150 mm i.d. (inner diameter), with a 1000-mm height, and the perforated distributor (with pore diameter of 2.0 mm and an open area ratio of 2.6%) is installed at the bottom. In the experiments, the particle mass was 2 kg and the height of initial static bed was about 100 mm. The bed wall is made of transparent Plexiglas thereby providing visual observation of the fluidization condition. On the wall of the bed column, a pressure probe, 50 mm in length and 4 mm i.d, was installed at four different heights (10, 90, 170, and 240 mm) above the distributor for signal collection. The pressure probe was connected to one of two input channels of differential pressure transducer (1151DP type, China), which produced output voltage proportional to the pressure difference between the two channels. The other channel was exposed to atmosphere. The measuring range of the pressure transducer is ± 5 kPa, and its relative accuracy is $\pm 0.1\%$ full scale. According to Shannon sampling theorem, sampling frequency must be twice higher than the highest frequency component of the signal. Thus, the sampling frequency was controlled at 200 Hz and the sampling time was 180 s.

The AE signal online collection and analysis system, developed by the UNILAB Research Center of Chemical Engineering at Zhejiang University, consists of an AE sensor, a preamplifier, a signal conditioning system, and a data acquisition system. The AE sensor used in this study is a piezoelectric accelerometer which is extensively used in collecting the acceleration of vibration without noise transferred via the air (PXR15, 150 kHz, 100–300 kHz, 65 dB, China). In the experiments, the AE sensor was attached closely to the outside wall of fluidized bed with silicone at a location of 90 mm above the gas distributor. The preamplifier (PXPA IV, 2–500 kHz, China) supplies sufficient gain to the AE signal to make sure it can be transmitted via a cable with length up to 200 m. The signal conditioning system used in our experiments is PXMA signal conditioning equipment (PXMA, China). It provides additional gain and filters to signals with a high-pass cutoff frequency of 2 Hz. The AE signals generated by piezoelectric accelerometer can be amplified and conditioned here. The data acquisition system in this study consists of a data acquisition card (NI PCI-6071E, National Instruments) and a personal computer. Finally, the signals are then transferred to the data acquisition card which is connected to the computer and controlled by software package LABVIEW. In these experiments, sampling frequency for AE signal was set as 500 kHz and its sampling time was 10 s.

In the study, cation exchange resin/water system was used as experimental material to keep density ratio nearly the same with that of industrial polyethylene/isopentane system. The cation exchange resin particle has a measured density of 1290 kg/m^3 and average diameter of 683 μm, and the particle size distribution was measured by a laser diffraction system (Malvern Mastersizer 2000), as shown in Figure 2. According to the Geldart classification, the resin is same with polyethylene, namely Geldart B type particle. The minimum fluidization gas velocity u_{mf} of this particle is 0.17 m/s. Air was used as the fluidizing gas with superficial gas velocity of 0.6 m/s and thus the fluidization number (v/u_{mf}) is 3.5. Water was sprayed into the reactor below the bed surface intermittently via a nozzle and the amount added was weighed accurately each time. The spraying location is shown in Figure 1. The addition of liquid destabilized the bed and it took several minutes for the bed to stabilize again.

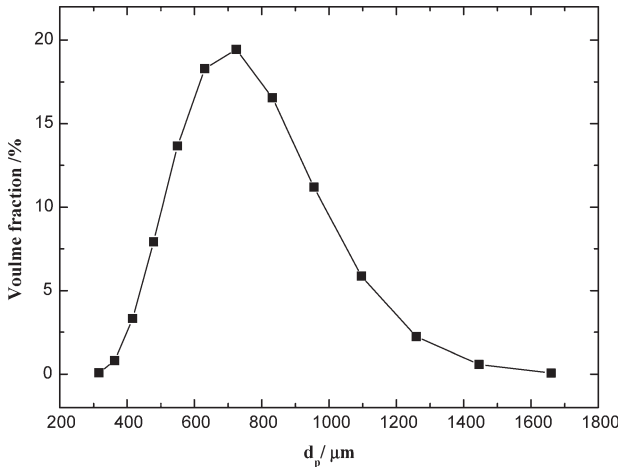

Figure 2. Particle size distribution of the cation exchange resin.

Once the bed stabilized, the pressure and AE signals were recorded. Through careful observation, it was noted that the added liquid content was almost constant during the fluidization. The mass of water lost during the experiment is shown in Table 1, from which we assume that the outlet gas is fully saturated during the process. In this article, pressure and AE signals were collected and analyzed under different particle/liquid mass ratio (m_l/m_s = 0, 0.08, 0.16, 0.24, 0.32, 0.4, 0.48, 0.56, 0.64, 0.72, 0.9) to study hydrodynamic characteristics of gas bubble and particle behavior in the fluidized bed.

Results and Discussions

Characterization of fluidization states by camera method

Figure 3 shows the fluidization states under different values of m_l/m_s and displays the fluidization characteristic change before and after the liquid addition. It can be obtained from Figure 3a that at $m_l/m_s = 0$, there is no liquid in the reactor, a large number of small bubbles exists in the fluidized bed and the bed shows a relatively even fluidization state. From Figure 3b, the addition of liquid leads to the emergence of large partial voidage zones (such as large bubbles) intermittently in the bed, which corresponds to the intermittency of particle motion. With the increase of liquid content (m_l/m_s>0.4) shown in Figure 3d, gas bubbles gradually become smaller while particle agglomerations start to appear near the bottom of the fluidized bed since the interaction forces between wetted particles have changed because of the liquid addition. As the liquid content continues to increase in the bed, as shown in Figure 3e, particle agglomerations aggravate, extending from the bottom to the remaining portion above the bed together with bubbles disappearing, which eventually lead to an obvious gas channeling in the bed.

Table 1. Mass Variation During the Experiment

Original Resin Particles (Before Fluidization)	Added Water	Ultimate Total Mass (After Fluidization)	Mass Variation (Water Leaving Column)
2.00 kg	1.80 kg	3.71 kg	0.09 kg (5%)

It should be pointed out that the liquid-containing gas–solid fluidized bed in the study is different with the traditional gas–liquid-solid three-phase fluidized bed in the sense that the water was adsorbed on particles surface instead of acting as a single phase, such as droplet or continuous phase.

Pressure fluctuation signals and gas bubble behavior

The Original Signals and Their Fluctuation. Figure 4 shows the original pressure fluctuation signals at 9-cm height above the distributor. From the top to the bottom of Figure 4, its sub-figures (a)–(f) represent the signals under different liquid content (m_l/m_s = 0, 0.08, 0.24, 0.4, 0.56, 0.9, respectively). When the fluidized bed was operated without liquid injection, the amplitude of pressure fluctuation was low and weak, which indicates that the gas bubbles were small and their activity intensity was relatively weak. As liquid was added to the fluidized bed, the pressure fluctuation signal witnessed an increase in amplitude and showed a certain regularity, which displays the same effect as that shown by intermittent large bubbles in Figure 3b. When the liquid content reached a certain level (m_l/m_s>0.4), the amplitude of the pressure fluctuation underwent a substantial drop, indicating an obvious bubble size reduction and then gas channeling. From then on, the pressure became stable and its fluctuation decreased gradually. This is because particles in the bed absorbed enough water, became saturated and then

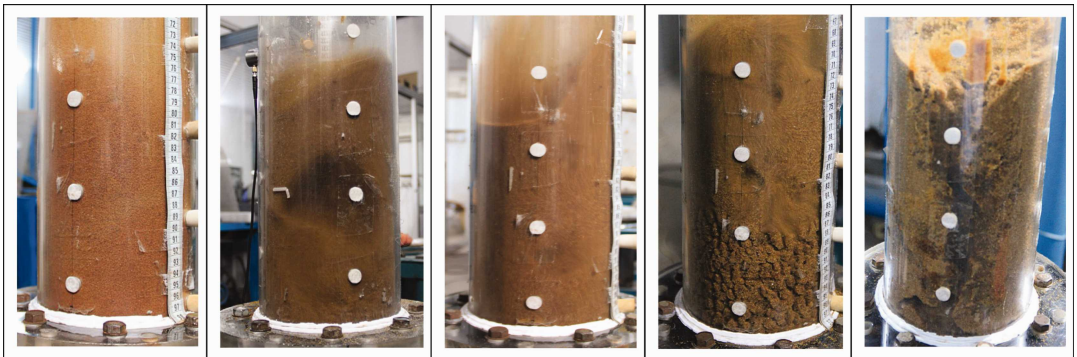

(a) $m_l/m_s = 0$	(b) $m_l/m_s = 0.24$	(c) $m_l/m_s = 0.4$	(d) $m_l/m_s = 0.56$	(e) $m_l/m_s = 0.9$

Figure 3. Fluidization states under different m_l/m_s (m_l/m_s represents liquid/solid mass ratio, referred as the same in the following).

[Color figure can be viewed in the online issue, which is available at wileyonlinelibrary.com.]

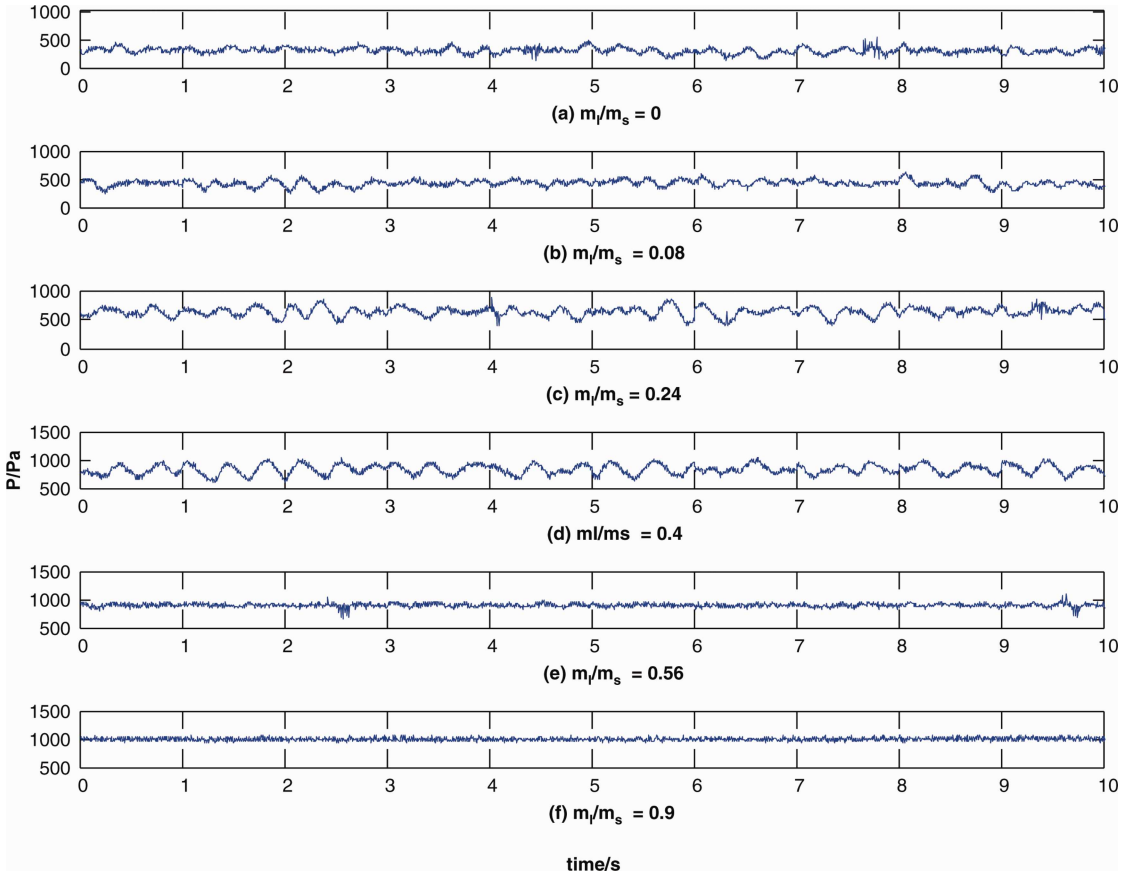

Figure 4. The original pressure signals under different m_l/m_s, at 9 cm above the distributor.

[Color figure can be viewed in the online issue, which is available at wileyonlinelibrary.com.]

stuck to each other, resulting in particle agglomerations, which limits gas bubbles motion and thus affects the pressure fluctuation signals in the fluidized bed. Besides, the liquid introduction led to the increase of the bed pressure, indicating the increase of the macroscopic dynamic bed level.

Standard Deviation Analysis and Bubble Size. In bubbling fluidized bed, gas bubbles interact with each other during the rising period, leading to bubbles coalescence or breakup. Meanwhile, pressure fluctuation signals will change accordingly and bubble size could be reflected via the amplitude and standard deviation of pressure fluctuation (σ_p).[15] By combining with the camera method, the bubble size variation can be deduced. Figure 5 shows the relationship between σ_p and m_l/m_s at various heights. When $m_l/m_s \leq 0.4$, there is no agglomerations in the fluidized bed. The σ_p increases with the value of m_l/m_s, which indicates that the bubbles are becoming larger in size at the same height. At $m_l/m_s = 0.48$, particle agglomerations start to form and become larger in the fluidized bed. The gas bubble size is limited and its activity restrained thus the value of σ_p drops rapidly. Gas channeling clearly appears in the bed ($m_l = 0.9$), and the value of σ_p decreases to the lowest, indicating that there is almost no bubbles existing in the fluidized bed, which shows the same result as that recorded by the camera. Through the above analysis, it can be concluded that the standard deviation of pressure fluctuation (σ_p) at each measurement height reflects the changes of gas bubble behavior and fluidization states. Therefore, σ_p can be used as a criterion to describe the quality of fluidization giving an insight into aspects such as particle agglomerations and gas channeling in the fluidized bed upon the addition of the liquid. Abnormal fluidization is observed once the value of σ_p drops rapidly after a sharp increase. From Figure 5, another conclusion can be made that the liquid content for agglomerates formation is different because of the difference in the measurement height. A larger liquid amount is needed for a higher measuring height.

Figure 5 further reveals that with the increase of the dynamic bed height, σ_p goes up first and then down before

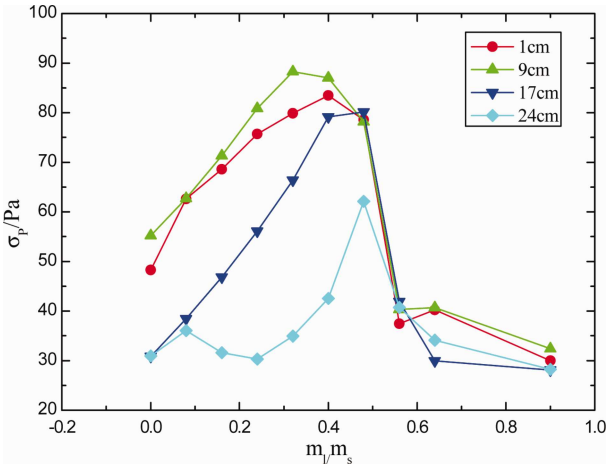

Figure 5. Relationship between σ_p of pressure and m_l/m_s at various heights.

[Color figure can be viewed in the online issue, which is available at wileyonlinelibrary.com.]

agglomerates take shape ($m_l/m_s \leq 0.4$), meaning that bubble size varies with bed height. When the agglomerates start to form ($m_l/m_s < 0.4$), σ_p drops to a lower level and the values of four curves in this figure are nearly the same, indicating that the gas bubbles for all heights become so small and disappear at last.

Power Spectrum Density Analysis and Bubble Motion Behavior. Power spectrum density (PSD) diagrams can be obtained using Fourier transformation to handle collected pressure signals. In these diagrams, the peak value represents the periodic component or random variable component and the peak frequency indicates the presence of gas bubbles of corresponding frequency.[27] Besides, the amplitude of pressure fluctuation shows the size of gas bubbles.[15] In the present work, the fast Fourier transformation algorithm was used to obtain the PSD diagrams of three different heights above fluidized bed distributor under different m_l/m_s, and at a gas velocity of 0.6 m/s, as shown in Figure 6.

From Figure 6a ($m_l/m_s = 0$), we know that the main frequency of the pressure fluctuation is about 4 Hz, indicating that the frequency of bubble formation is also about 4 Hz. With the increase of height above distributor, gas bubbles coalesce into larger ones or break up during their rising period. Therefore, low-frequency components increase at higher heights. Because of the fact that measurement position was at the bed level, it was observed that there were few particles above the probe, hence such a signal is formed in the third plot of Figure 6a. As m_l/m_s increases to 0.24 (Figure 6b), signal amplitude near the main frequency is significantly enhanced, illustrating that the bubbles become larger and thus their motion becomes active. Meanwhile, the dynamic bed level increases from 16 to 22 cm, so a remarkable power spectrum at the height of 17 cm appears in Figure 6b, indicating formation of gas bubbles in the higher positions of the fluidized bed. When m_l/m_s continually rises to 0.48 (Figure 6c), the added liquid causes particle agglomerations and thus represses the bubble behavior, making the size of the bubbles inside the fluidized bed decrease. Therefore, the PSDs at three different heights together experience modest drops in amplitude. As the liquid content continues to increase to $m_l/m_s = 0.9$ (Figure 6d), particle agglomerations are aggravated, leading to gas channeling in the fluidized bed. From Figure 3d, we can see that there are no gas bubbles in the fluidized bed, which indicates that the PSD with very low frequency component results from the gas channeling rather than gas bubbles. From the above discussions, we can conclude that with the cumulative increase in the liquid content, the gas bubbles in the fluidized bed increase at first, then decrease and eventually disappear. It is clear that the PSDs can reflect bubble size change and corresponding activity of bubbles during the liquid-adding process.

The gas (in form of gas bubble) is the main energy source of particle fluidization in fluidized beds. Its behavior was characterized with the help of the pressure measurement technique in the present work. Through the analysis of such behavior, information of the bubble movement can be obtained. Although, particle behavior is the direct embodiment of fluidization characteristics in fluidized beds, its characterization is also crucial. In light of research progress of AE measurement related to particle motion,[11,19,28,29] the particle motion behavior and its overall flow behavior will be studied by the AE technique as well as different analytic methods in the following sections.

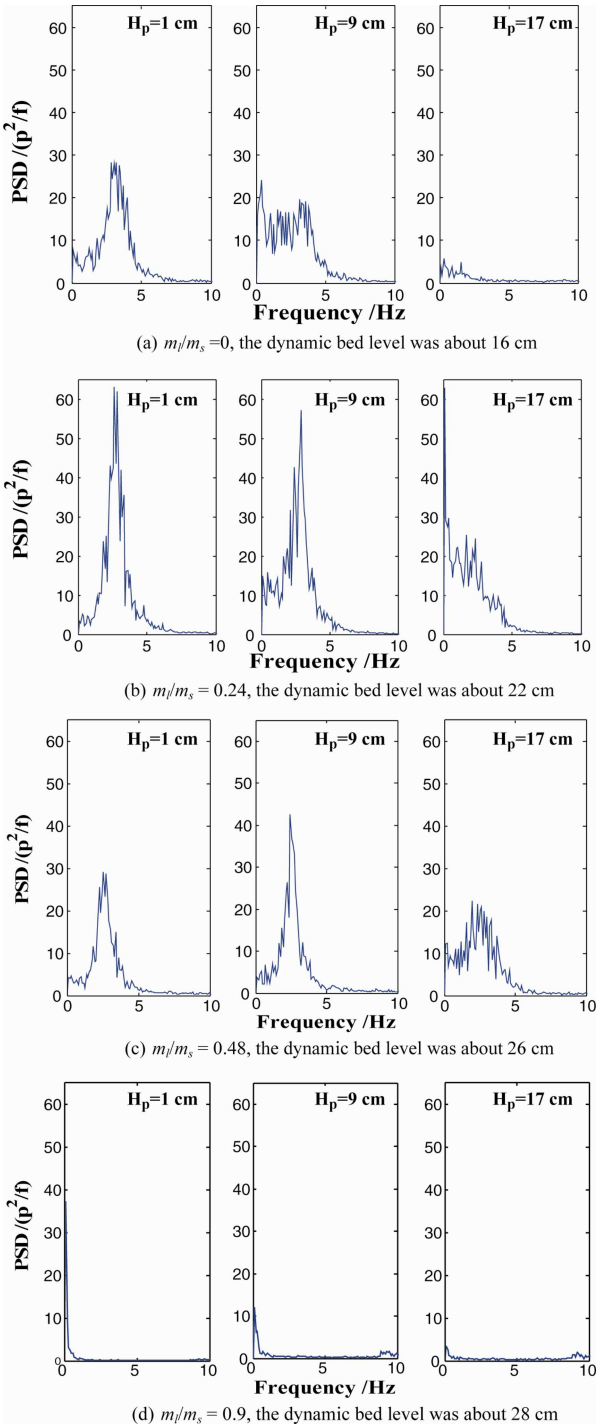

(a) m_l/m_s =0, the dynamic bed level was about 16 cm

(b) m_l/m_s = 0.24, the dynamic bed level was about 22 cm

(c) m_l/m_s = 0.48, the dynamic bed level was about 26 cm

(d) m_l/m_s = 0.9, the dynamic bed level was about 28 cm

Figure 6. PSD diagrams of pressure fluctuation with different m_l/m_s at various heights.

[Color figure can be viewed in the online issue, which is available at wileyonlinelibrary.com.]

AE signals and particle behavior

AE Energy Analysis and Particle Motion. AE signals can reflect particle motion well in fluidized beds.[19,26,29,30] Figure 7 shows the average energy of AE in the fluidized bed under different liquid content at a height of 9 cm above the distributor. At first, the AE energy presents an upward trend with the increase of liquid ($0 < m_l/m_s \leq 0.24$), indicating that the particle motion becomes active, and at $m_l/m_s = 0.24$, its activity is most acute which is consistent with above PSD

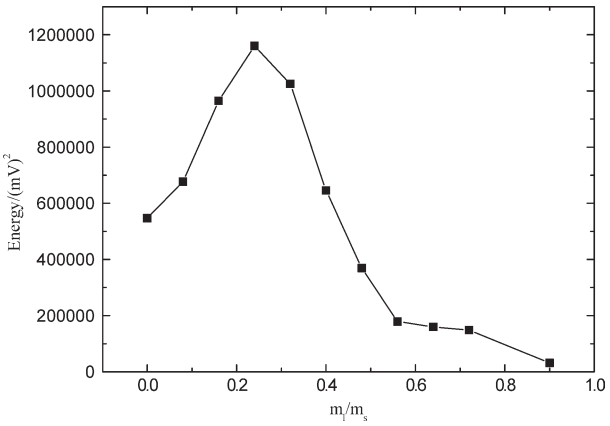

Figure 7. The relationship between AE energy and m_l/m_s at 9 cm above the gas distributor.

results of the pressure fluctuation. It is well-known that solid mixing in gas–solid fluidized bed is caused by gas bubbles passing through the bed, and its mixing degree depends on the number and size of the gas bubbles. Therefore, the particle motion should agree with the changing tendency of the gas bubbles, which was verified by our measurement results. When the liquid content reaches to $m_l/m_s = 0.32$, the AE energy starts to decline from an upward trend. It means the intensity of the particle motion becomes lower, which is consistent with that of the gas bubble motion according to the PSD results. With the liquid continuously increasing, the energy reduces significantly to a steady low level at $m_l/m_s = 0.56$. This is because particle agglomerates formed near and at the measurement height (9 cm above the gas distributor) blocked the bubble motion as well as the corresponding particle motion. Therefore, the AE energy value on the curve remains constant since then. Gradually, the particle agglomerates spread in the entire bed, leading to an overall defluidization of the bed. Meanwhile, the gas bubbles disappear and gas channeling flow is formed. These two factors cause a small energy decrease at $m_l/m_s = 0.9$. The results of the above acoustic energy analysis are verified by the four pictures in Figure 3 which also clearly reflects the overall changes of fluidization states in the bed.

Wavelet Analysis and Particle Size Change. Energy spectrum of different scales can be obtained by wavelet decomposing of acoustic signals. Such spectrum can be then used to characterize particle motion of different size so as to realize the measurement for particle size distribution in fluidized beds.[20,31,32] Previous research shows that through wavelet decomposing of acoustic signals, different scale signals can be obtained. Among these signals, the lower scale components represent high frequency signal, standing for the acoustic energy of small particle motion. Although, the higher scale parts represent low frequency signal, standing for that of the large particle motion.

By applying seven scales wavelet analysis to the AE signals, the energy percentage diagrams of different scales can be obtained as shown in Figure 8. The x-coordinate of each picture stands for wavelet scale, the number 1 to 7 on the x-coordinate for different detail signals and the number 8 for approximation signal. In Table 1, the d^1–d^7 components represent detail signals from first to seventh scale after wavelet decomposition and a^7 represents approximation signal of the seventh scale. The frequency range for each wavelet scale is clearly shown in Table 2. Similar to the relevant analysis methods in Ref. [31], in this experimental system, d^1–d^3 wavelet scales (high frequency) represent relatively small particle motion and the d^4–d^6 scales (low frequency) represent large particle motion. It is clear from the figure that with the increase of the liquid content, the energy percentage of d^1–d^3 scales decreases whereas that of d^4–d^5 scales increases gradually, indicating the decrease of small particle content and the increase of large particle content. This is because in the whole liquid-adding process, the bed viscosity becomes enhanced with the increase of liquid content, and thus small

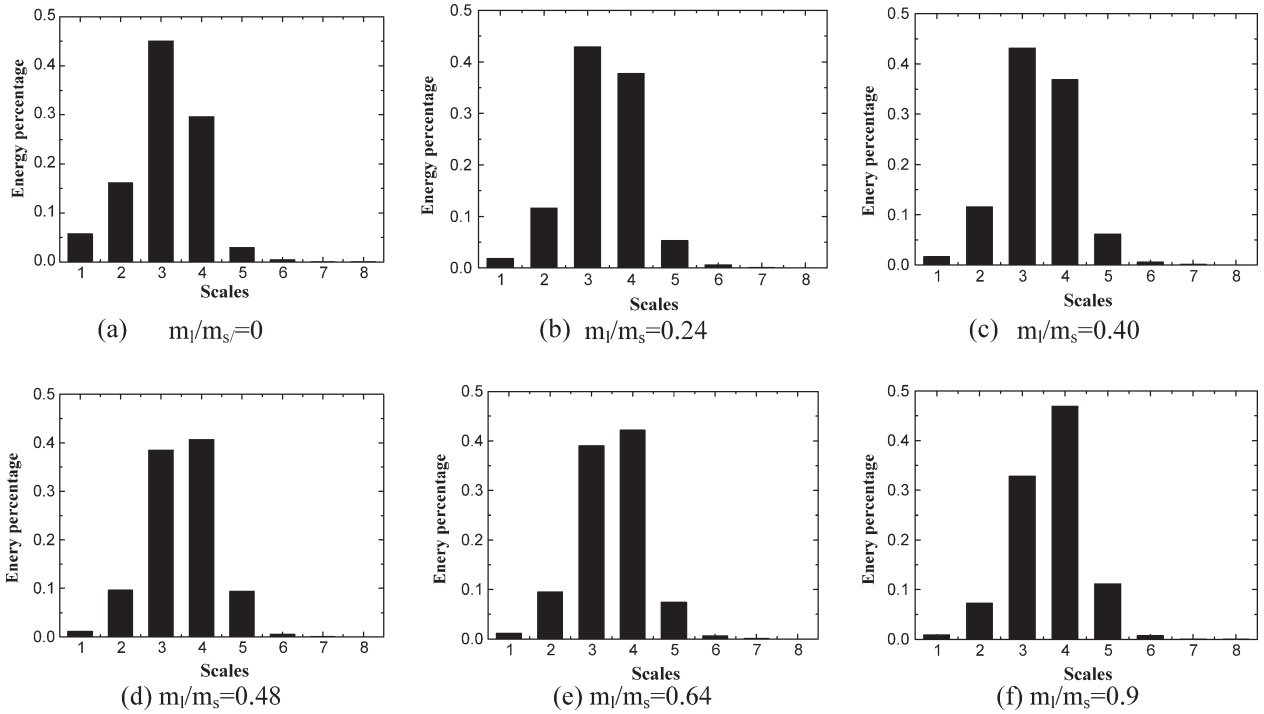

Figure 8. The AE energy percentage of various scales with different m_l/m_s.

Table 2. The Corresponding Frequency Range of Various Levels After seven-scale Wavelet Decomposition

Scales	d^1	d^2	d^3	d^4	d^5	d^6	d^7	a^7
Frequencies (kHz)	125–250	62.5–125	31.2–62.5	15.6–31.2	7.8–15.6	3.9–7.8	2.0–3.9	0–2.0

particles connected together and bonded into large ones due to the "bridge" built by the added liquid.[33] Especially, at $m_l/m_s = 0.48$, the wavelet energy distribution of different scales changes greatly with a substantial growth in energy percentage of d^4 and d^5. Such a growth may be caused by the significant change in the activity of gas bubbles. However, the energy percentage of scale d^6–d^7, a^7 is low and remains unchanged, which means there was little particle movement of corresponding frequency in the experiment. Figures 3 obtained using camera method have already demonstrated that there indeed exists a particle size change during the liquid-adding process, which, at the same time, also verifies the positive results of AE measurements.

Cycle Detection in the Liquid-Adding Process. ***Hurst analysis.*** Hurst analysis, also called R/S analysis, is a method to quantify persistence of time series[34] and has been successfully applied in many multiphase systems.[17,26,35–38] The related specific mathematical algorithm and the implementation details of this analysis can be found in this reference.[26] In short, Hurst analysis divides time series into time intervals of length τ and calculates the rescaled range values. The average can be computed for all intervals τ. Changing the value of interval length τ, the Hurst exponent H for the curve of interval can be estimated through the slope of the $\lg(R/S)$ and $\lg(\tau)$ plot, which can be obtained by following formula

$$R(t,\tau)/S(t,\tau) \propto \tau^H \tag{1}$$

where R is the range (extreme difference) and S is the standard deviation of acoustic signal sequence, respectively. According to Peters,[39] if the time series exhibits cyclic behavior, the Hurst exponent H would vary at specific values of the interval length τ and the shape of $\lg(R/S)$ vs. $\lg(\tau)$ plot is not a straight line. The x-coordinate of the break in this plot refers to the cycle time. Moreover, the number of cyclic component is the same as the break number on the line. Besides, the constant value of H means noncyclic component of the signal.

Figure 9 shows an AE signal plot of $\lg(R/S)$ vs. $\lg(\tau)$ under different liquid content. From this figure, we can get that the τ of this main break point is 0.0158 *ms* (from $\lg\tau = -4.8$) indicating the main cycle time is 0.0158 *ms* and the reciprocal of the point between the two linear regions is about 63.1 kHz which is close to the dominant frequency of the signal. These results are consistent with the reference.[40] According to the above wavelet analysis, we can see that the above mentioned dominant frequency (high frequency) component and its cyclic behavior can reflect particle motion. From Figure 9, we can see that at $m_l/ms = 0.48$, there is a new clear break in the $\lg(R/S) \sim \lg\tau$ curve between points $\lg\tau = -3$ and $\lg\tau = -2$, which indicates that the new periodic signal (with a cycle time of 2.5 *ms* and corresponding frequency of about 400 Hz) appeared in the fluidized bed at relatively high delay time when the liquid was introduced. This cyclic behavior at this frequency can be ascribed to the cluster motion or bubble motion.[26] A reasonable explanation for the occurrence of the signal is that the addition of the liquid resulted in the agglomeration of particles, then led to the periodicity of the impact produced by particle agglomeration on the wall and the interaction between the gas bubbles. The new break was thus gradually formed with the increase of the liquid content. Therefore, we can infer such a clear break could be used as a criterion to judge whether or not abnormal fluidization state (such as particle agglomerations and gas channeling) occurs in the fluidized bed during the liquid-adding process. In this figure, the break between the points $\lg\tau = -3$ and $\lg\tau = -2$ indicates the emergence of the abnormal fluidization.

V-statistics analysis. Peters[39] proposed the V-statistics as a further tool to detect cyclic behavior. The V-statistics improves Hurst's rescaled range analysis, using a "peak" instead of a "break" in the $\lg(R/S)$ vs. $\lg(\tau)$ curve for its easier recognition on the premise that the break is between a section of slope H larger than 0.5 and a section of slope smaller than 0.5, and the V-statistics analysis is defined as follow

$$V_\tau = \frac{(R/S)_\tau}{\sqrt{\tau}} \tag{2}$$

Figure 10 represents the V-statistics plot under different liquid content. It is another different expression for the content of Figure 9 and is easier to detect cyclic time. Compared with Hurst analysis in Figure 9, the V-statistics analysis results shown in Figure 10 can reflect the signal cyclic properties and its corresponding cycle time more clearly. By the use of this figure, new cyclic behavior (of agglomeration collision and bubble motion) caused by the addition of liquid in the system could be fully displayed and the occurrence of particle agglomeration could also be identified by the emergence of the "peak." From Figure 10, we can see that there are two evident peaks on each curve. In the V-statistics

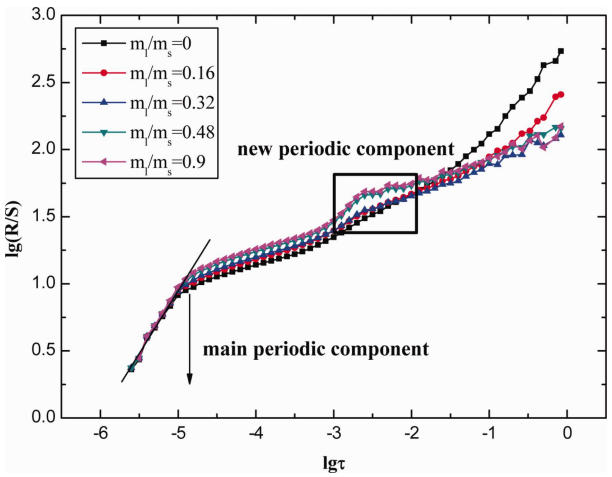

Figure 9. The $\lg(R/S)\sim\lg\tau$ plot of AE signal under different liquid content.

[Color figure can be viewed in the online issue, which is available at wileyonlinelibrary.com.]

analysis, the peak value (V_{max}) can reflect the intensity of cyclic behavior. To be specific, the greater the V_{max},, the more intense the cyclic behavior.[41] By calculation, V_{max} under different liquid content can be obtained and plotted as shown in Figure 11. In this figure, the curves V_{max1} and V_{max2} correspond to the maximum values of V-statistics in the first cyclic behavior and the second-cyclic behavior respectively, and two curves present the similar change trend. We attempt to explore the relationship between V_{max} and the liquid content in details. According to above PSD analysis of the pressure fluctuation, the bubble size and its activity in the fluidized bed would increase significantly at the beginning of the liquid addition process ($0 \leq m_l/m_s \leq 0.16$), resulting in the intensification of corresponding cyclic behavior of gas bubbles. According to classical bubble wake mechanism, the particle mixing is mainly caused by the wake of rising bubbles, which enhances the cyclic behavior of these particles. Therefore, V_{max} increases correspondingly in this period. When m_l/m_s is increased from 0.16 to 0.4, little change of cyclic behavior of bubbles and particles is observed. As a result, V_{max} is almost constant under this circumstance. However, when m_l/m_s is increased further to 0.48 or higher, the hydrodynamic behavior in the fluidized bed undergoes significant changes—some abnormal fluidization phenomena occurs, such as particle agglomeration, reduction of bubble size and quantity as well as emergence of gas channeling. All these abnormal phenomena together results in a new cyclic behavior in the bed. Therefore, V_{max} correspondingly starts to experience a sharp growth at $m_l/m_s = 0.48$ and keeps an increasing trend after that. Through the above analysis, with regard to the liquid content, the trend of V_{max} in Figure 11 is in accordance with that of "breaks" in Figure 9. To be specific, the added liquid results in new cyclic behavior (break) as well as the increase of V_{max}. V_{max} experiences a sharp increase at a critical liquid to solid ratio (for example at $m_l/m_s = 0.48$), it indicates that the abnormal fluidization occurred in the fluidized bed, such as agglomeration or gas channeling, which was verified by the camera and pressure fluctuation analysis. Therefore, we can draw a conclusion that the variation of V_{max} could be also used as a criterion to judge whether or not abnormal fluidization state occurs in the fluidized bed. Compared to the criterion "the break" in the R/S analysis (Figure 9), the criterion V_{max} obtained from V-statistics analysis (Figure 11) gives a much better picture of the situation and can be detected more easily, and thus can be used to judge the occurrence of unsteady fluidization phenomena more accurately.

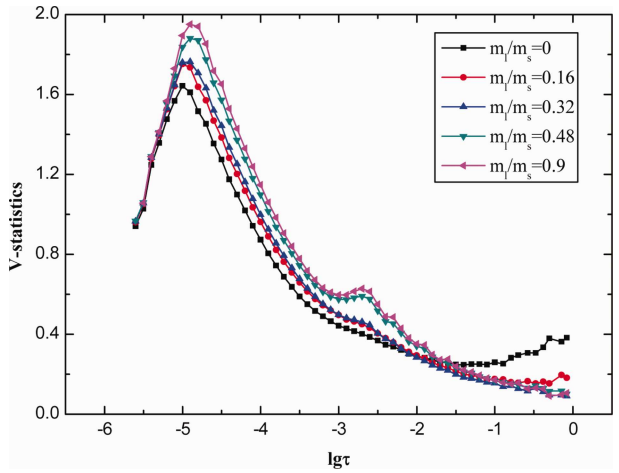

Figure 10. *V*-statistics plot of AE signal for different liquid content.

[Color figure can be viewed in the online issue, which is available at wileyonlinelibrary.com.]

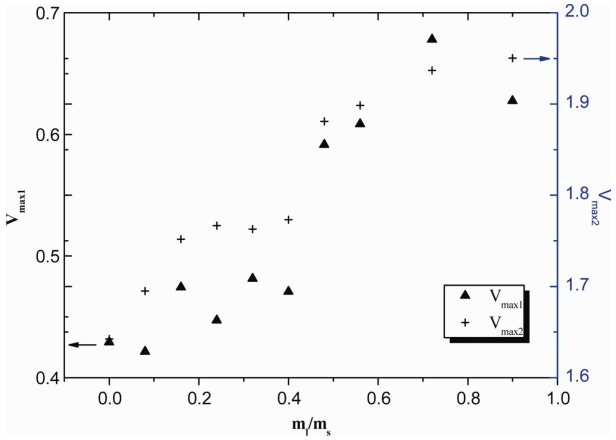

Figure 11. Evolution of two kinds of V_{max} values under different liquid content.

[Color figure can be viewed in the online issue, which is available at wileyonlinelibrary.com.]

Conclusions and highlights

Addition of a liquid phase into a gas–solid fluidized bed significantly alters the hydrodynamic behavior of the fluidized bed. To verify this point by sufficient and comprehensive fluidization information, the present work investigated the changes of hydrodynamic behavior and fluidization state in the liquid-containing fluidized bed thoroughly by means of camera, pressure and acoustic techniques. Different measurement techniques were applied in the research to enable a comprehensive study of different targets (such as particles, gas bubbles, and overall fluidization states) in this multiphase flow system. Through careful experiment and detailed analysis, the main findings of the study can be summarized as follows:

(1) As pressure fluctuation measurement is suitable for the study of gas bubbles in the fluidized bed, it has been applied in this work to investigate the changes of gas bubble size and corresponding bubble motion. Results of original signal, standard deviation and PSD analysis of the pressure fluctuation demonstrate that when the liquid was continuously added into the fluidized bed, the gas bubbles in the bed underwent a transition in dominating distribution form from small bubbles to large bubbles at first, and then the bubbles became smaller, and disappeared at last. Meanwhile, the gas bubble movement showed a similar changing trend with the bubble size. Through systematic analysis, a conclusion can be drawn that the standard deviation σ_p of the pressure fluctuation can be used as a criterion to determine whether or not abnormal fluidization phenomenon (such as particle agglomeration or gas channeling) occurs in the fluidized bed when the added liquid was increased.

(2) As a promising measuring technique used in fluidized beds, the AE measurement shows overwhelming advantages in particle characterization. The acoustic average energy can reflect the particle motion process in the bed clearly, which agrees with the bubble motion process measured by pressure fluctuation. However, the acoustic technique reveals more

information about hydrodynamics, such as the change of particle diameter, the occurrence of new cyclic behavior. By applying wavelet analysis to AE signals, it was observed that small particles in the bed display a tendency to become larger ones by combining with each other, which cannot be detected through pressure fluctuation measurement. Besides, the Hurst and V-statistics analysis methods are both used to identify new periodic behavior of the signals during the liquid-adding process. Further, it has been proved that the break formation and the change in the trend of V_{max} are caused. The two methods could thus be also used as criteria to detect the occurrence of abnormal fluidization phenomenon.

What's more, the camera method was also applied to characterize the changes of overall fluidization states and verified the results of pressure and acoustic measurements. Therefore, we came to the conclusion that the said three techniques together can reflect hydrodynamics in the fluidized bed comprehensively.

From an industrial perspective, the pressure and acoustic measurements could be widely applied in plant-scale FBRs due to their relatively easy implementation. It would beneficial for industrial detection (such as gas bubble properties and particle motion measurements) to combine the two measuring techniques successfully. Because of such great industrial significance, the research of this paper deserves further study.

To sum up, the main results of this article show that when the liquid content kept at a lower level in the fluidized bed, the gas bubbles became larger and their movement was strengthened. The particle activity was also getting more intense. It is favorable for fluidization in the fluidized bed. However, as the liquid continued to increase, gas bubbles turned to become smaller and gradually disappeared. The interaction among these gas bubble weakened correspondingly, causing the reduction of fluidization quality at the same time inducing the defluidization in the bed, which is detrimental to industrial production.[42] Therefore, we can draw a key conclusion from this article that in industrial operation, liquid added to the FBR must be strictly controlled so as to meet requirement for heat removal in the meantime keep fluidization in a normal state. In a word, this work can provide certain theoretical guidance for industrial liquid-containing operation processes.

Acknowledgments

The work is supported by National Natural Science Foundation of China (Grant No. 21076180), National Basic Research Program of China (2012CB720500), Specialized Research Fund for the Doctoral Program of Higher Education (20110101120020) and Fundamental Research Funds for Central Universities (2011QNA4032).

Literature Cited

1. Tsujimoto H, Yokoyama T, Huang CC, Sekiguchi I. Monitoring particle fluidization in a fluidized bed granulator with an acoustic emission sensor. *Powder Technol*. 2000;113:88–96.
2. McDougall S, Saberian M, Briens C, Berruti F, Chan E. Effect of liquid properties on the agglomerating tendency of a wet gas-solid fluidized bed. *Powder Technol*. 2005;149:61–67.
3. McDougall S, Saberian M, Briens C, Berruti F, Chan E. Using dynamic pressure signals to assess the effects of injected liquid on fluidized bed properties. *Chem Eng Process*. 2005;44:701–708.
4. Weber S, Briens C, Berruti F, Chan E, Gray M. Agglomerate stability in fluidized beds of glass beads and silica sand. *Powder Technol*. 2006;165:115–127.
5. Weber S, Briens C, Berruti F, Chan E, Gray M. Effect of agglomerate properties on agglomerate stability in fluidized beds. *Chem Eng Sci*. 2008;63:4245–4256.
6. Book G, Albion K, Briens L, Briens C, Berruti F. On-line detection of bed fluidity in gas-solid fluidized beds with liquid injection by passive acoustic and vibrometric methods. *Powder Technol*. 2011; 205:126–136.
7. Vervloet D, Nijenhuis J, van Ommen JR. Monitoring a lab-scale fluidized bed dryer: a comparison between pressure transducers, passive acoustic emissions and vibration measurements. *Powder Technol*. 2010;197:36–48.
8. McLaughlin LJ, Rhodes MJ. Prediction of fluidized bed behaviour in the presence of liquid bridges. *Powder Technol*. 2001;114:213–223.
9. Seville JPK, Clift R. The effect of thin liquid layers on fluidization characteristics. *Powder Technol*. 1984;37:117–129.
10. Wormsbecker M, Pugsley T, Tanfara H. Interpretation of the hydrodynamic behaviour in a conical fluidized bed dryer. *Chem Eng Sci*. 2009;64:1739–1746.
11. Boyd JWR, Varley J. The uses of passive measurement of acoustic emissions from chemical engineering processes. *Chem Eng Sci*. 2001;56:1749–1767.
12. van Ommen JR, Mudde RF. Measuring the gas-solids distribution in fluidized beds—a review. *Int J Chem React Eng*. 2008;6:1–32.
13. van Ommen JR, Sasic S, van der Schaaf J, Gheorghiu S, Johnsson F, Coppens M-O. Time-series analysis of pressure fluctuations in gas-solid fluidized beds—a review. *Int J Multiphase Flow*. 2011; 37:403–428.
14. Werther J. Measurement techniques in fluidized beds. *Powder Technol*. 1999;102:15–36.
15. Bi HT. A critical review of the complex pressure fluctuation phenomenon in gas-solids fluidized beds. *Chem Eng Sci*. 2007;62:3473–3493.
16. Johnsson F, Zijerveld RC, Schouten JC, van den Bleek CM, Leckner B. Characterization of fluidization regimes by time-series analysis of pressure fluctuations. *Int J Multiphas Flow*. 2000;26:663–715.
17. Zhao GB, Yang YR. Multiscale resolution of fluidized-bed pressure fluctuations. *AIChE J*. 2003;49:869–882.
18. Zhou YF, Dong KZ, Zhengliang H, Wang JD, Yang YR. Fault detection based on acoustic emission-early agglomeration recognition system in fluidized bed reactor. *Ind Eng Chem Res*. 2011;50:8476–8484.
19. Wang JD, Ren CJ, Yang YR, Hou LX. Characterization of particle fluidization pattern in a gas solid fluidized bed based on acoustic emission (AE) measurement. *Ind Eng Chem Res*. 2009;48:8508–8514.
20. Jiang XJ, Wang JD, Jiang BB, Yang YR, Hou LX. Study of the power spectrum of acoustic emission (AE) by accelerometers in fluidized beds. *Ind Eng Chem Res*. 2007;46:6904–6909.
21. Allan P, Bellamy LJ, Nordon A, Littlejohn D. Non-invasive monitoring of the mixing of pharmaceutical powders by broadband acoustic emission. *Analyst*. 2010;135:518–524.
22. Cao YJ, Wang JD, He YJ, Liu W, Yang YR. Agglomeration detection based on attractor comparison in horizontal stirred bed reactors by acoustic emission sensors. *AIChE J*. 2009;55(12):3099–3108.
23. Abbasi A, Sotudeh-Gharebagh R, Mostoufi N, Zarghami R, Mahjoob MJ. Nonintrusive characterization of fluidized bed hydrodynamics using vibration signature analysis. *AIChE J*. 2010;56:597–603.
24. de Martín L, Villa Briongos J, Aragón JM, Palancar MC. Can low frequency accelerometry replace pressure measurements for monitoring gas-solid fluidized beds? *Chem Eng Sci*. 2010;65:4055–4064.
25. de Martín L, Briongos JV, García-Hernando N, Aragón JM. Detecting regime transitions in gas-solid fluidized beds from low frequency accelerometry signals. *Powder Technol*. 2010;207:104–112.
26. He YJ, Wang JD, Cao YJ, Yang YR. Resolution of structure characteristics of ae signals in multiphase flow system-from data to information. *AIChE J*. 2009;55:2563–2577.
27. Park SH, Kang Y, Kim SD. Wavelet transform analysis of pressure fluctuation signals in a pressurized bubble column. *Chem Eng Sci*. 2001;56:6259–6265.
28. Abbasi M, Sotudeh-Gharebagh R, Mostoufi N, Mahjoob MJ. Non-intrusive monitoring of bubbles in a gas-solid fluidized bed using vibration signature analysis. *Powder Technol*. 2009;196:278–285.
29. Cody GD, Johri J, Goldfarb D. Dependence of particle fluctuation velocity on gas flow, and particle diameter in gas fluidized beds for monodispersed spheres in the Geldart B and A fluidization regimes. *Powder Technol*. 2008;182:146–170.
30. Cody GD, Goldfarb DJ, Storch GV, Norris AN. Particle granular temperature in gas fluidized beds. *Powder Technol*. 1996;87:211–232.
31. Ren CJ, Wang JD, Song D, Jiang BB, Liao ZW, Yang YR. Determination of particle size distribution by multi-scale analysis of acoustic emission signals in gas-solid fluidized bed. *J Zhejiang Univ-Sci A*. 2011;12:260–267.

32. Chen X, Chen D. Measuring average particle size for fluidized bed reactors by employing acoustic emission signals and neural networks. *Chem Eng Technol*. 2008;31:95–102.
33. Mikami T, Kamiya H, Horio M. Numerical simulation of cohesive powder behavior in a fluidized bed. *Chem Eng Sci*. 1998;53:1927–1940.
34. Hurst HE. Long-term storage capacity of reservoirs. *Am Soc Civil Eng*. 1950;76:1–30.
35. Bai D, Issangya AS, Grace JR. Characteristics of gas-fluidized beds in different flow regimes. *Ind Eng Chem Res*. 1999;38:803–811.
36. Briens CL, Briens LA, Hay J, Hudson C, Margaritis A. Hurst's analysis to detect minimum fluidization and gas maldistribution in fluidized beds. *AIChE J*. 1997;43:1904–1908.
37. Briens LA, Briens CL. Cycle detection and characterization in chemical engineering. *AIChE J*. 2002;48:970–980.
38. Ferrante L, Miccio M, Miccio F, Solimene R. Fluidized bed combustion of liquid biofuels: application of integrated diagnostics for micro-explosions characterization. *Energy Fuel*. 2008;22: 4213–4222.
39. Peters EE. *Applying Chaos to Investment and Economics*. New York: Wiley, 1994.
40. Fan LT, Kang Y, Neogi D, Yashima M. Fractal analysis of fluidized particle behavior in liquid-solid fluidized beds. *AIChE J*. 1993;39: 513–517.
41. Ariyapadi S, Berruti F, Briens C, Knapper B, Skwarok R, Chan E. Stability of horizontal gas-liquid sprays in open-air and in a gas-solid fluidized bed. *Powder Technol*. 2005;155:161–174.
42. DeChellis ML, Griffin JR. Inventors: exxon chemical patents, Inc, assignee. Process for polymerizing monomers in fluidized beds. US Patent 5352749; 1994.

Manuscript received Sept. 4, 2011, and revision received Jun. 12, 2012.